TRENDS IN SCIENCES 2026; 23(5): 11876
https://doi.org/10.48048/tis.2026.11876 RESEARCH ARTICLE

Temperature-Dependent Microstructure and Lattice Distortion in Pure Magnesium Investigated by Neutron and X-ray Diffraction

Muhammad Rifai[1], Muhammad Ivan Pratama[2], Azza Alifa Muhammad[1], Ahadi Damar Prasetya[3], Mujamilah[3], Frida Iswinning Diah[1], Agus Dwiatmaja[1], Fajar Sidik Permana[1], Kurnia Wibowo[4], Suharni[1], Taufik[1], Emy Mulyani[1] and Ihwanul Aziz[1,*]

[1]Research Center for Accelerator Technology, Research Organization for Nuclear Energy, National Research and Innovation Agency of Indonesia (BRIN), Banten 15314, Indonesia
[2]Metallurgical Engineering, Faculty of Engineering, Universitas Sultan Ageng Tirtayasa, Banten 42435, Indonesia
[3]Research Center for Nuclear Beam Analysis Technology, Research Organization for Nuclear Energy, National Research and Innovation Agency of Indonesia (BRIN), Banten 15314, Indonesia
[4]Directorate for Laboratory Management, Research Facilities, and Science and Technology Park, Deputy for Research and Innovation Infrastructure, National Research and Innovation Agency of Indonesia (BRIN), Jakarta Pusat 10340, Indonesia

([*]Corresponding author's e-mail: ihwa002@brin.go.id)

Received: 12 September 2025, Revised: 6 October 2025, Accepted: 16 October 2025, Published: 1 January 2026

Abstract

This study investigates the microstructural evolution and residual stress behavior of pure magnesium processed by Accumulative Roll Bonding (ARB) at 250 and 350 °C for up to 4 cycles. Characterization using Optical Microscopy, SEM, XRD, and Neutron Diffraction revealed significant grain refinement, with the smallest grain size of 6.591 μm in the Mg 3A sample (250 °C, 3 cycles). XRD indicated texture evolution with enhanced (002) orientation and increased lattice strain (0.21816%), while neutron diffraction confirmed compressive residual stress, reaching 138.275 MPa in Mg 3A. Lower processing temperature promoted finer grains and higher residual stress, whereas higher temperature facilitated recovery and stress relaxation. The combined use of XRD and neutron diffraction provided complementary insights into surface and bulk changes. Unlike conventional approaches that rely solely on XRD, this study uniquely integrates neutron diffraction to probe bulk stresses, marking a novel contribution in the characterization of ARB-processed pure magnesium. This approach represents a novel contribution in characterizing ARB-processed pure magnesium. ARB at 250 °C for 3 cycles was identified as the optimal condition to enhance microstructure and manage residual stress in pure magnesium.

Keywords: Pure magnesium, Accumulative roll bonding, Microstructural evolution, Lattice distortion, Neutron diffraction, Residual stress

Introduction

Magnesium, one of the lightest structural metals, has attracted significant attention due to its exceptional strength-to-weight ratio and its potential applications in sectors such as transportation, aerospace, and electronics [1-3]. With a density approximately 2/3 that of aluminum [4], magnesium presents a compelling case for lightweight engineering solutions aimed at improving fuel efficiency, reducing carbon emissions, and enhancing mechanical performance in load-sensitive environments [5-7]. However, despite these attractive features, its broader industrial adoption has been limited by several inherent drawbacks. These include low ductility at room temperature, poor

formability, and a high tendency to develop residual stress and texture-related mechanical anisotropy [8,9]. These issues pose challenges in both manufacturing and performance reliability, especially in structural or cyclic loading applications.

One of the principal strategies to overcome these material limitations involves grain refinement, a method aimed at enhancing the strength and ductility of metals through structural control at the microscopic level [10-12]. Grain refinement improves mechanical properties by impeding dislocation motion and modifying deformation behavior, particularly in hexagonal close-packed (HCP) structures like magnesium, which naturally exhibit limited slip systems [13]. Among various grain refinement techniques, Severe Plastic Deformation (SPD) methods have emerged as highly promising [14-16]. These include Equal Channel Angular Pressing (ECAP) [17], High-Pressure Torsion (HPT) [18], and Accumulative Roll Bonding (ARB) [19,20]. ARB, has gained interest due to its scalability for industrial application, simple tooling, and ability to process sheet metals into ultrafine-grained materials without significantly altering the external geometry of the sample.

ARB, in particular, is attractive due to its simple tooling, scalability, and capability to produce ultrafine-grained sheets through repeated stacking, rolling, and bonding at 50% thickness reduction per cycle [19,21,22]. Through this repetitive rolling, it becomes possible to accumulate large strains while maintaining the original shape of the specimen. This makes ARB suitable for producing bulk ultrafine-grained materials with enhanced mechanical properties.

The microstructure of magnesium is a critical determinant of its mechanical behavior. Grain size, orientation, and boundary character influence yield strength, fatigue resistance, and corrosion susceptibility [23,24]. For instance, finer grains generally correspond to higher strength through the Hall-Petch relationship, while uniform grain distribution may reduce stress concentrations and delay crack initiation. Additionally, the crystallographic texture, or preferred grain orientation, plays a pivotal role in the deformation mechanics of HCP metals, where basal slip is dominant [13]. Any SPD technique applied to magnesium must not only refine the grain size but also account for the resulting texture evolution. Without control over texture, improvements in strength may come at the cost of ductility or formability, properties equally essential for practical applications [25,26].

Temperature is another significant factor influencing ARB outcomes. Higher processing temperatures promote dynamic recovery and recrystallization, which may alleviate residual stresses and allow for more uniform deformation [27-29]. However, excessive recovery may also counteract the grain refinement process by enabling grain growth, particularly if thermal exposure is prolonged or repeated [30-32]. On the other hand, lower processing temperatures tend to suppress recovery, promoting higher dislocation density and stronger textures, albeit with a risk of crack formation and brittleness. Identifying a temperature range that balances these competing effects is essential for optimizing the ARB process in magnesium. A key concern that arises during SPD is the development of residual stress, a form of internal stress retained within the material after plastic deformation. In magnesium, which has low stacking fault energy and a high propensity for twinning, the magnitude and distribution of residual stresses can significantly affect long-term structural integrity [33,34]. Compressive residual stresses may improve fatigue life by retarding crack propagation, while tensile stresses may have the opposite effect, accelerating failure.

Understanding how ARB influences residual stress in different temperature and strain conditions is, therefore, fundamental for designing components that are both strong and durable. To evaluate these effects, advanced characterization techniques are required. While X-ray Diffraction (XRD) has been widely used to study crystallographic changes, its penetration depth is limited to the material's surface [13,35,36]. The novelty of this work lies in integrating XRD with neutron diffraction to capture both surface and volumetric strain evolution, offering the first comprehensive correlation of ARB processing parameters with bulk residual stress in pure magnesium. Consequently, it provides only partial information, especially when dealing with bulk stress states. Neutron Diffraction offers a non-destructive method capable of probing deep within the material, allowing for a more accurate assessment of internal strain and stress distributions. Combining both techniques yields a more holistic understanding of how

the internal structure of magnesium evolves during and after ARB processing [37]. However, understanding how ARB influences microstructure and residual stress in pure magnesium remains limited. Conventional surface-sensitive XRD provides only partial information, as it cannot capture volumetric stresses. To address this gap, this study integrates XRD with neutron diffraction, enabling a multi-scale characterization of both surface and bulk structural evolution, an approach rarely applied in ARB studies of magnesium.

This study uniquely integrates surface-sensitive XRD with bulk-probing neutron diffraction to capture both lattice distortion and volumetric residual stress. This dual-scale characterization, rarely applied in ARB studies of magnesium, provides new insights into microstructure–stress relationships and offers practical guidelines for optimizing ARB parameters.

Materials and methods

Sample preparation

The experimental procedure commenced by cutting pure magnesium ingots into plate specimens measuring 150× 33×2.2 mm^3 using a mechanical shear cutter. To eliminate any microstructural alterations induced by machining, the plates were annealed at 400 °C for 1 h in a Carbolite muffle furnace, followed by furnace cooling for 24 h to ensure homogenization. Initial sample characterization involved microstructural observation and residual stress measurement. Surface preparation began with mechanical grinding using a Metkon Forcipol 2V grinding machine equipped with 100-grit SiC sandpaper. The specimens were then cleaned with analytical-grade acetone in an ultrasonic bath to remove any surface contaminants such as oil or debris.

ARB processing

For ARB processing, 2 magnesium plates were stacked and secured together with copper wire. A bench drill was used to perforate the plates at both edges to ensure mechanical bonding during rolling. Pre-heating for ARB was performed at either 250 or 350 °C in the same muffle furnace for 25 min. These temperatures were selected to represent 2 critical regimes in magnesium processing: 250 °C, where recovery is limited and dislocation accumulation promotes strong grain refinement, and 350 °C, where increased thermal activation facilitates dynamic recovery and stress relaxation. Rolling was conducted using a 2-high laboratory rolling mill (Fujita RM-30) operating at a roll speed of 26 revolutions per minute under a roll load of approximately 10 tons. Each ARB cycle involved a 50% thickness reduction, yielding an equivalent strain (ε) of 0.8 per cycle. The number of ARB cycles applied was varied from 1 to 4. Four cycles were chosen as the upper limit because prior studies and preliminary trials indicated that beyond this point grain refinement tends to saturate and recovery or coarsening becomes dominant, making additional cycles less effective.

Material characterization

Microstructural characterization was performed using an Olympus BX51M Optical Microscope (OM) and a JEOL JSM-6510LV Scanning Electron Microscope (SEM). Grain size was measured based on OM images using the ImageJ software (NIH, USA), following ASTM E112. Phase identification and lattice strain analysis were carried out using a PANalytical X'Pert Pro X-ray Diffractometer equipped with Cu Kα radiation (λ = 1.5406 Å). XRD data were analyzed with HighScore Plus software, enabling precise evaluation of peak intensity and crystallographic orientation changes. Residual stress was measured using 2 methods. For surface-level stress, the SmartSite RS Portable X-ray Stress Analyzer (Rigaku) was employed using the $\sin^2\psi$ method. For internal stress profiling, neutron diffraction measurements were conducted following ISO/TS 21432:2005 standards, providing non-destructive and volumetric stress data. Sample codes and processing conditions are detailed in **Table 1**.

Table 1 Sample code system.

Sample Code	Temperature (°C)	Number of ARB Cycles	Description
Mg 0	400 (annealed)	0	Reference (as-annealed)
Mg 1A	250	1	1 cycle at 250 °C
Mg 2A	250	2	2 cycles at 250 °C
Mg 3A	250	3	3 cycles at 250 °C
Mg 4A	250	4	4 cycles at 250 °C
Mg 1B	350	1	1 cycle at 350 °C
Mg 2B	350	2	2 cycles at 350 °C
Mg 3B	350	3	3 cycles at 350 °C
Mg 4B	350	4	4 cycles at 350 °C

Results and discussion

This study investigates the microstructural evolution and internal strain behavior of pure magnesium subjected to Accumulative Roll Bonding (ARB) at 2 different temperatures, 250 and 350 °C. The characterization was performed using a combination of Optical Microscopy (OM), Scanning Electron Microscopy (SEM), X-ray Diffraction (XRD), and Neutron Diffraction techniques to elucidate the material's response to severe plastic deformation. The as-annealed pure magnesium sample (Mg 0) exhibited clear grain boundaries with an average grain size of 145.593 µm, as observed in **Figure 1** and documented in **Table 2**. OM and SEM confirmed the presence of relatively coarse grains with well-defined morphology, which served as the reference for post-ARB microstructural comparison. These grains represented the initial condition of the material prior to deformation, setting a critical baseline for assessing the impact of ARB on microstructure and internal stress.

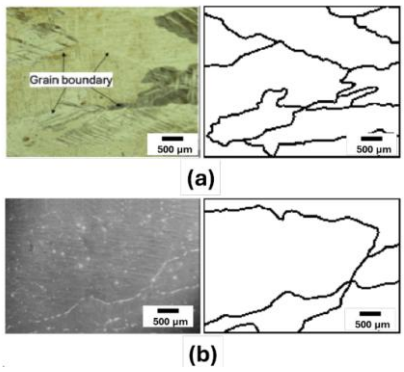

Figure 1 Results of Microstructure Observation of Mg (pure) As annealed: (a) OM and (b) SEM.

Table 2 Pure magnesium grain size data before and after ARB process.

Sample Code	Average Grain Size (µm)
Mg 0	145.593
Mg 1A	23.404
Mg 2A	12.557
Mg 3A	6.591
Mg 4A	9.182
Mg 1B	36.369
Mg 2B	17.913
Mg 3B	9.575
Mg 4B	10.479

Grain size decreased from Cycle 1 to Cycle 3 at both temperatures, reaching a minimum of 6.6 μm at 250 °C (Mg 3A) and 9.6 μm at 350 °C (Mg 3B). At Cycle 4, grain coarsening occurred in both cases, but the effect was more pronounced at 350 °C. Grouping by temperature clearly shows that 250 °C sustained finer grains across all cycles compared to 350 °C, confirming the stronger suppression of recovery at lower temperature.

The microstructural evolution of pure magnesium processed by Accumulative Roll Bonding (ARB) under different thermal and cycle conditions is demonstrated through optical and scanning electron micrographs, as shown in **Figures 2** to **4**. In the OM images presented in **Figure 2**, the microstructure after 1 ARB cycle at 250 °C exhibits prominently elongated grains aligned along the rolling direction, indicating the accumulation of directional plastic strain. In comparison, the sample processed at 350 °C displays more equiaxed and rounded grains, which suggests that the elevated temperature facilitates dynamic recovery and inhibits excessive grain elongation. **Figure 3** presents SEM micrographs of ARB-processed magnesium at 250 °C (a - d) and 350 °C (e - h) for cycles 1 - 4. To improve clarity, the images could be reorganized into 2 rows - 250 °C (a - d) and 350 °C (e - h)-with corresponding cycles shown side by side. This would make the progression across cycles and the comparison between temperatures more evident. The current differences between subfigures are not very distinct; higher-quality images with clearer annotations, or selected higher-magnification views, would better highlight features such as slip traces, subgrain formation, and boundary mobility. Despite these limitations, the overall trend is clear: lower temperature favors elongated, strain-hardened grains, while higher temperature promotes equiaxed grains through enhanced recovery and recrystallization. Further insights are provided in **Figure 3**, where the microstructures following 1 to 4 ARB cycles are compared for both temperatures. At 250 °C, grain refinement progresses notably through Cycle 3, where the smallest grain size is recorded. However, by Cycle 4, signs of grain coarsening emerge, implying that continued deformation leads to recovery or recrystallization. At 350 °C, the grains remain predominantly equiaxed across all cycles. Although some refinement occurs up to Cycle 3, a reversal in this trend is observed in Cycle 4, where grains grow larger due to increased thermal activation, promoting stress relaxation and boundary migration. High-resolution SEM images in **Figure 4** confirm these trends after the fourth ARB cycle. The microstructure at 250 °C still reveals elongated grains with localized relaxation zones, indicating the onset of microstructural stabilization. Meanwhile, the sample processed at 350 °C shows more homogeneous and equiaxed grains, reflecting a more advanced state of thermal recovery and recrystallization. These observations collectively demonstrate that ARB temperature and cycle number critically influence grain morphology, strain accumulation, and recovery behavior in pure magnesium. The coarse grains in the annealed state reflect a low initial dislocation density and thermally stabilized microstructure. This condition provides a useful baseline to evaluate how ARB introduces high defect density and subgrain structures that progressively evolve with strain accumulation.

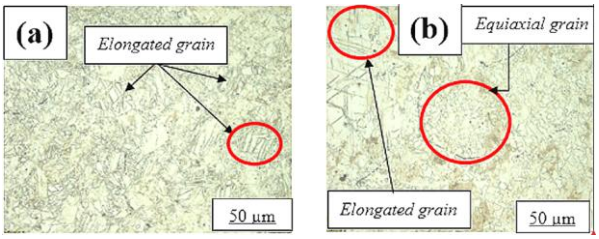

Figure 2 Optical micrographs of pure Mg after 1 ARB cycle: (a) 250 °C showing elongated grains along rolling direction due to suppressed recovery, and (b) 350 °C showing more equiaxed grains indicating enhanced dynamic recovery.

The refinement observed up to Cycle 3 is consistent with the accumulation of dislocations and their rearrangement into subgrain boundaries, which eventually transform into high-angle grain boundaries. This mechanism leads to progressive grain subdivision until strain saturation occurs. By Cycle 4, the stored

energy from accumulated defects promotes boundary migration and recovery processes. At 250 °C, limited recovery allows partial coarsening, while at 350 °C, higher thermal activation facilitates more extensive recovery and dynamic recrystallization. These processes explain why refinement reaches a limit and transitions into coarsening beyond the third cycle.

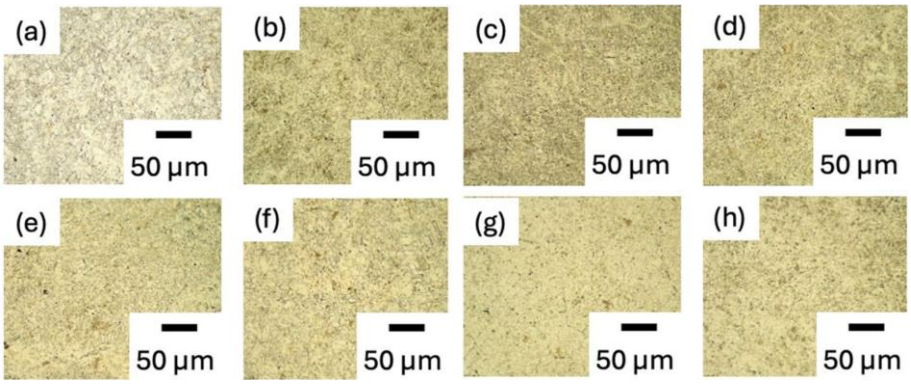

Figure 3 Optical micrographs of Mg after ARB at 250 and 350 °C for 1 - 4 cycles: (a - d) 250 °C samples show progressive grain refinement up to cycle 3 (minimum grain size), followed by grain coarsening at cycle 4 due to recovery; (e - h) 350 °C samples remain equiaxed across cycles with moderate refinement and subsequent grain growth at cycle 4.

Figure 5(a) further illustrates the relationship between ARB cycles and average grain size. A decreasing trend was observed from cycle 1 to cycle 3, followed by a modest increase at cycle 4. This non-linear trend in grain size evolution suggests that while ARB effectively refines grains through severe plastic deformation, extended processing may initiate grain growth due to strain-induced boundary migration or static recovery effects. Meanwhile, **Figure 5(b)** presents the evolution of residual stress, showing that compressive stresses increase progressively up to cycle 3 and then decrease at cycle 4. This trend reflects the balance between strain hardening and recovery/recrystallization mechanisms. Error bars are included in the plot to indicate measurement variability, and the relatively small standard deviations confirm the reliability of the data. The peak compressive stress observed at 250 °C after 3 cycles suggests that this condition maximizes dislocation density and lattice distortion before recovery becomes dominant. Lower temperature (250 °C) proved more effective in sustaining grain refinement, with smaller average grain sizes compared to 350 °C, emphasizing the role of suppressed thermal energy in impeding grain coarsening. **Figure 6** confirms the significance of ARB process temperature in determining magnesium's average grain size. Lower temperatures favor grain refinement, while higher temperatures lead to grain growth. These insights are instrumental in fine-tuning the ARB process to optimize pure magnesium materials' microstructural qualities and performance.

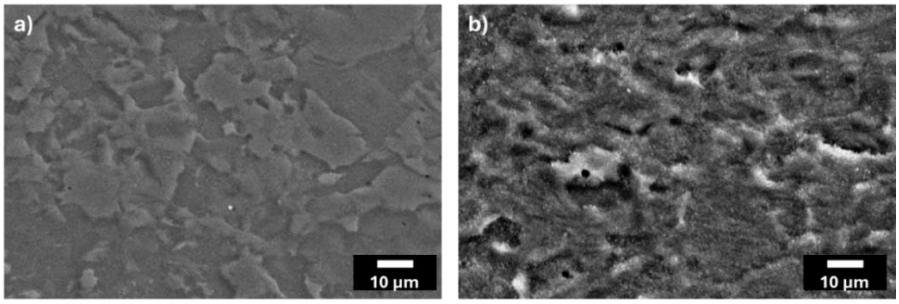

Figure 4 SEM images of Mg after 4 ARB cycles: (a) 250 °C showing elongated grains with localized relaxation zones, and (b) 350 °C showing equiaxed grains reflecting advanced recovery and recrystallization.

X-ray diffraction analysis provided essential insight into the crystallographic texture and lattice strain of the material. **Figures 6(a)** and **6(b)** display XRD patterns of magnesium samples processed at 250 and 350 °C, respectively. The as-annealed sample exhibited sharp diffraction peaks, with a dominant intensity around 34.365°, corresponding to the (002) plane of the HCP magnesium structure. After ARB, the XRD patterns demonstrated notable broadening and peak intensity alterations, indicative of grain refinement, increased dislocation density, and evolving crystallographic orientation. Specifically, the (002) peak intensity increased slightly post-ARB, while peaks corresponding to the (011) and (012) planes showed a decline and shift, highlighting a texture transformation favoring basal plane alignment. A new significant peak at 47.772°, associated with the (012) orientation, emerged with increasing ARB cycles, confirming texture evolution due to rolling-induced strain. The elongated grains observed at 250 °C are indicative of high dislocation storage and limited recovery, consistent with deformation-driven subgrain formation. In contrast, equiaxed grains at 350 °C suggest enhanced boundary mobility and dynamic recrystallization, which counteract the accumulation of deformation texture. The grain coarsening at higher cycles, particularly at 350 °C, can be attributed to boundary migration facilitated by thermal activation. The reduction in grain size up to cycle 3 is consistent with dislocation subdivision and the formation of high-angle boundaries. The subsequent grain growth in cycle 4 reflects strain-induced boundary migration and recovery, where accumulated stored energy drives coarsening rather than further refinement.

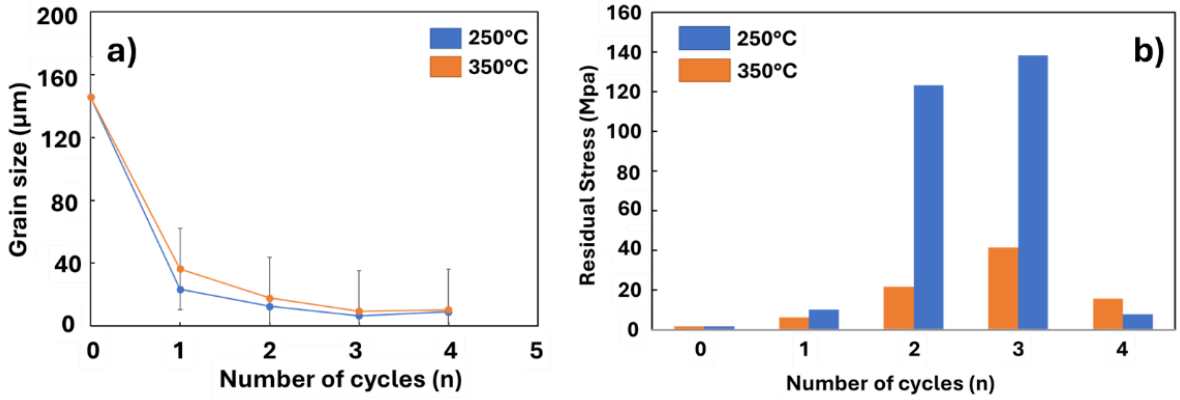

Figure 5 Graph of the effect of number of ARB cycles on grain size of pure magnesium (a), effect of number of ARB cycles on pure magnesium residual stress (b).

Lattice strain values, extracted from the XRD peak broadening and detailed in **Table 3**, offered further evidence of internal stress evolution during ARB. At 250 °C, the lattice strain peaked during the third cycle (0.21816%), aligning with the minimum grain size and highest dislocation density. The increasing trend in strain until the third cycle, followed by a drop at cycle 4, suggests strain saturation and potential relaxation phenomena. At 350 °C, a similar trend was observed, though strain values remained slightly lower, confirming the role of thermal energy in facilitating dislocation recovery. This data supports the assertion that ARB at lower temperatures enhances lattice strain, promoting microstructural refinement, whereas higher temperatures contribute to stress relaxation and grain stabilization.

The peak broadening and intensity changes not only reflect refinement but also increased dislocation density. The decline in lattice strain after cycle 3 suggests partial recovery, possibly through dislocation annihilation and subgrain coalescence at elevated strain energy states. XRD revealed peak broadening and basal (002) texture strengthening with ARB. Lattice strain rose until cycle 3 (max. 0.218%), then relaxed at cycle 4, consistent with dislocation saturation and recovery. Strain levels were lower at 350 °C, confirming enhanced thermal recovery.

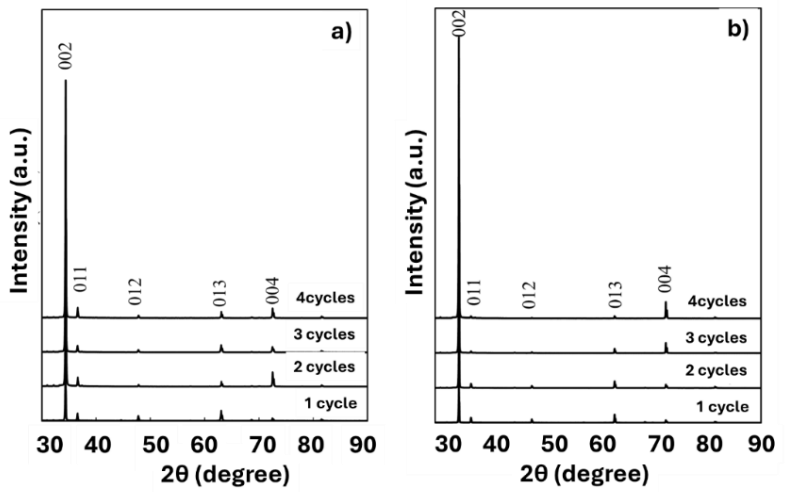

Figure 6 XRD patterns of Mg after ARB: (a) 250 °C showing stronger basal (002) orientation and higher lattice strain, and (b) 350 °C showing broader peaks with reduced strain due to recovery.

Table 3 Lattice strain value.

Cycle	Lattice Strain (%)	
	250 °C	**350 °C**
0	0	0
1	0.19464	0.15457
2	0.19436	0.14458
3	0.21816	0.18198
4	0.15449	0.15458

Lattice strain increased with cycles up to Cycle 3, then relaxed at Cycle 4. At 250 °C, strain reached 0.218% in Mg 3A, while at 350 °C the peak was lower (0.182% in Mg 3B). Grouping the results by temperature highlights that lower processing temperature consistently produced higher strain, reflecting greater dislocation density and reduced recovery. The peak strain at cycle 3 reflects a state of maximum dislocation density and subgrain formation, where further plastic deformation no longer generates significant new defects but instead accumulates stored energy. By cycle 4, part of this stored energy is released through recovery mechanisms such as dislocation annihilation and subgrain coalescence, reducing the overall lattice distortion. At 350 °C, the earlier onset of recovery leads to a lower maximum strain, consistent with enhanced thermal activation of dislocation motion.

Neutron diffraction, was utilized to examine the internal strain across various orientations. Measurements were taken in normal, axial, and transverse directions to obtain a comprehensive understanding of strain distribution. The neutron wavelength was set at 1.718 Å, and using Bragg's law and appropriate elastic constants (E = 45 GPa, ν = 0.29), lattice strain was computed from diffraction peak shifts. **Figure 7** presents a comparison of residual stress distributions derived from X-ray techniques, showing notable differences across temperatures and cycles. The anisotropy in strain distribution detected by neutron diffraction, especially at 250 °C in cycle 4, indicates heterogeneous recovery and localized recrystallization. This highlights the competing mechanisms of strain hardening and recovery, which govern the final stress state and texture development.

For the Mg 1A sample (250 °C, 1 cycle), neutron diffraction results indicated consistently negative strain values in all orientations, signifying uniform compressive deformation. This result demonstrates that even a single ARB cycle at a relatively low temperature is effective in inducing grain refinement and compressive lattice distortion. In contrast, the Mg 4A sample (250 °C, 4 cycles) exhibited more complex

behavior. While compressive strain was still dominant, positive values emerged in the normal direction, suggesting the initiation of localized grain coarsening or strain recovery. These changes signify that extended deformation may induce anisotropic strain distribution, possibly due to texture sharpening or microstructural instability. Neutron diffraction confirmed compressive strain in early cycles, stronger at 250 °C. By cycle 4, strain became anisotropic, reflecting texture sharpening and localized recovery. At 350 °C, residual stresses were weaker, indicating greater stress relaxation.

At 350 °C, the Mg 1B and Mg 4B samples retained compressive strain across all orientations, although the magnitude was lower than in the 250 °C counterparts. This result aligns with expectations that higher processing temperatures facilitate dislocation movement and partial stress relaxation. Notably, the evolution of strain patterns across cycles revealed a gradual decline in residual strain, suggesting that ongoing deformation progressively redistributes internal stresses, potentially stabilizing the microstructure.

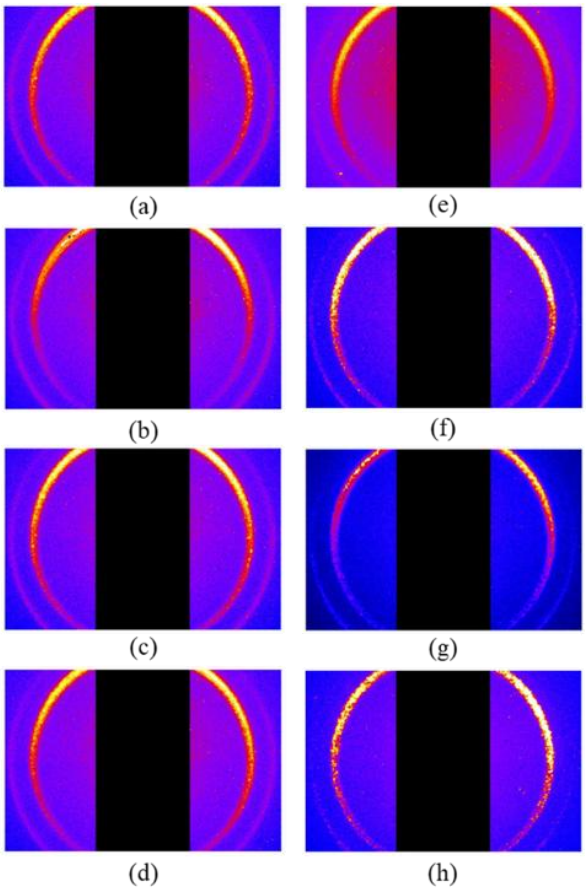

Figure 7 Neutron diffraction residual stress analysis of ARB-processed Mg: (a - d) 250 °C samples show increasing compressive stress up to cycle 3, with partial relaxation at cycle 4; (e - h) 350 °C samples exhibit lower compressive stress, reflecting enhanced stress relaxation at higher temperature.

The pronounced peak in residual stress at cycle 3 corresponds to the highest stored strain energy and densest dislocation network, which produces strong compressive stress fields. In the fourth cycle, boundary migration and partial recrystallization provide pathways for stress redistribution, leading to stress relaxation. This explains the reduction in residual stress despite continued deformation. The contrast between 250 and 350 °C further demonstrates how temperature governs the balance between strain hardening and recovery, with lower temperatures favoring defect storage and higher temperatures accelerating relaxation.

The correlation between XRD-derived lattice strain and neutron-detected residual strain highlights the complementary nature of these 2 techniques. XRD, with its surface sensitivity and high angular resolution,

provided insights into peak broadening and lattice distortion near the sample surface. In contrast, neutron diffraction allowed for a volumetric assessment of internal strain, revealing spatial variations and texture alignment in 3 dimensions. Together, these methods provided a holistic view of how ARB influences magnesium's microstructure and stress state. Moreover, residual stress analysis based on X-ray measurements confirmed that lower ARB temperatures yielded higher residual stresses. For example, at the third cycle, residual stress in Mg 3A exceeded 138 MPa, whereas in Mg 3B it was approximately 41 MPa. This suggests that low-temperature processing not only increases strain but also promotes the accumulation of internal stress, which may have implications for the mechanical behavior and corrosion susceptibility of the material. Mechanistically, the accumulation of high compressive residual stress can retard crack initiation and slow down corrosion pit growth by suppressing tensile stress fields that normally accelerate localized dissolution. However, when residual stress becomes highly heterogeneous, as observed at cycle 4, local tensile pockets may emerge and act as preferential sites for galvanic activity, thereby increasing susceptibility to stress-corrosion cracking. The balance between compressive strengthening and the risk of localized tensile stresses is therefore crucial in determining the long-term corrosion performance of ARB-processed magnesium. In line with previous studies on ECAP-processed AZ31 alloys, residual stress levels were found to be higher at lower processing temperatures, corroborating the findings of this study. This association is attributed to greater dislocation densities and reduced recovery at lower temperatures, which hinder stress relaxation and enhance the material's hardness and strength. Finally, the analysis of crystallographic orientation using neutron diffraction revealed that ARB affects not only grain size and residual strain but also texture evolution. Comparable findings have been reported in previous SPD studies on magnesium alloys. For instance, ECAP-processed AZ31 showed enhanced residual stress at lower processing temperatures, directly linked to high dislocation density and limited recovery. Similarly, ARB studies on AZ31 and AZ91 alloys confirmed that cyclic deformation at reduced temperature accelerates grain refinement while sustaining compressive residual stress. The present results on pure Mg align with these observations, reinforcing the idea that suppressed dynamic recovery is the dominant mechanism. By contextualizing our findings with earlier SPD literature, it becomes evident that ARB at 250 °C for up to 3 cycles represents an optimal balance between grain refinement, stress accumulation, and microstructural stability, consistent with trends reported in other Mg-based alloys. Preferred alignment along the (004) and (021) planes was observed in ARB-processed samples, particularly after 3 cycles. This texture development is associated with improved mechanical anisotropy and is essential for tailoring the material's performance in structural applications. Identifying 250 °C with 3 ARB cycles as the optimal condition has direct significance for structural applications. At this point, the microstructure reaches its finest grain size, residual stress is maximized in a compressive state, and lattice strain is elevated without triggering instability. These combined features are beneficial for lightweight structural components because compressive residual stress can enhance fatigue life, refined grains improve yield strength, and controlled texture alignment reduces the risk of premature failure. In practice, this means that magnesium processed under these conditions could serve more reliably in load-bearing or cyclic environments, such as automotive panels, aerospace structures, and portable electronics housings, where both strength-to-weight ratio and dimensional stability are critical.

The results from OM, SEM, XRD, and neutron diffraction techniques collectively demonstrate that the ARB process effectively refines grain structure, alters crystallographic orientation, and modulates residual stress in pure magnesium. These effects are highly dependent on processing temperature and the number of cycles applied. Lower temperatures favor greater refinement and strain accumulation, while higher temperatures contribute to stress relaxation and grain stabilization. The combination of XRD and neutron diffraction provides a powerful toolkit for comprehensively characterizing these structural changes, guiding the optimization of ARB parameters for future applications in lightweight, high-strength materials.

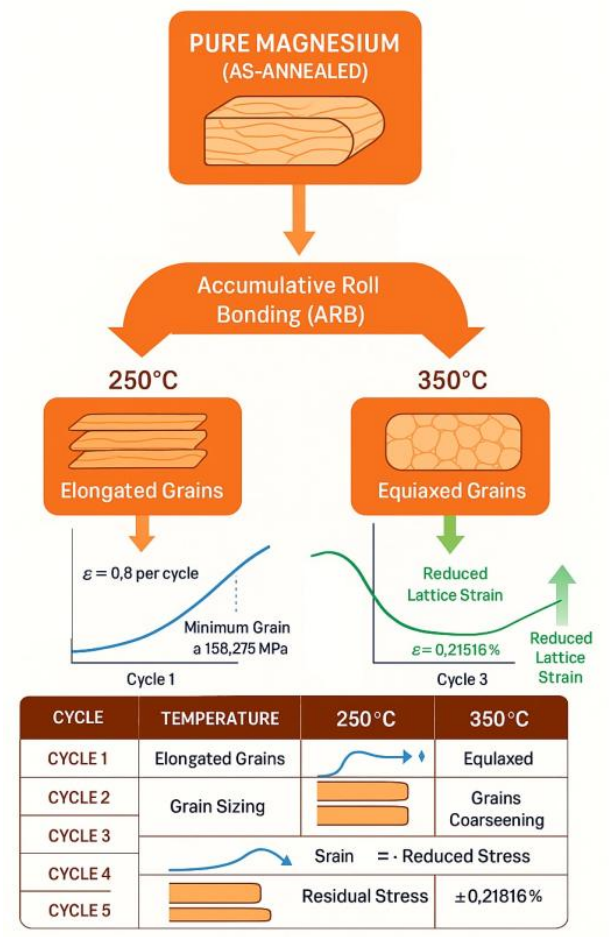

Figure 8 Microstructural and stress response of pure magnesium under ARB processing at varying temperatures.

The observations from this study provide a detailed view of how the ARB process influences the microstructure, crystallographic orientation, and residual stress of pure magnesium. The combined use of OM, SEM, XRD, and Neutron Diffraction has enabled a comprehensive understanding of the microstructural evolution and internal strain behavior of the material. The novelty of this study lies in demonstrating how neutron diffraction complements XRD: while XRD revealed lattice distortion and peak broadening near the surface, neutron diffraction captured 3-dimensional internal stress distributions. This combined methodology not only validates the results but also sets a precedent for future SPD studies on lightweight metals. **Figure 8** summarizes the combined microstructural and stress responses of pure magnesium under ARB. The refinement observed up to the third cycle at 250 °C represents the optimal balance between dislocation accumulation and limited recovery, while the coarsening seen at cycle 4 highlights the onset of boundary migration and partial recrystallization. More importantly, this figure emphasizes the processing window that maximizes both refinement and compressive stress-conditions directly relevant to improving mechanical reliability in structural applications. Specifically, maintaining finer grains while retaining compressive residual stress suggests enhanced fatigue resistance and reduced susceptibility to crack initiation. Thus, rather than simply illustrating grain size evolution, **Figure 8** provides a practical guideline: ARB at 250 °C for 3 cycles offers the best trade-off between strength and stability for lightweight magnesium components.

The morphology of the grains also changed significantly depending on the processing temperature. At 250 °C, grains became elongated along the rolling direction, reflecting the directional nature of strain under constrained deformation. Conversely, at 350 °C, the grains remained more equiaxed, a result of increased thermal activation which facilitates dislocation

annihilation and grain boundary mobility. These differences underscore the role of temperature in governing the balance between strain hardening and recovery during ARB. X-ray diffraction patterns revealed pronounced changes in crystallographic orientation due to ARB. Initially, the diffraction peaks were sharp and reflected a relatively random grain orientation. After ARB, the (002) basal plane peak intensified, indicating preferential alignment along this direction. Furthermore, the emergence of a new dominant peak at 47.772° (associated with the (012) plane) signaled a reorientation of grains due to rolling strain. This development of texture, particularly the dominance of the (002) and (012) orientations, is characteristic of HCP materials like magnesium subjected to rolling. Such orientation changes are critical because they influence the anisotropy of mechanical properties, affecting the material's performance in structural applications.

The analysis of lattice strain derived from XRD showed that the internal distortion of the crystal lattice increased up to the third ARB cycle, then decreased. The highest strain value recorded was 0.21816% at 250 °C in the third cycle. This trend implies that while initial deformation accumulates strain and promotes dislocation density, extended cycling allows for some relaxation, possibly via dynamic recovery. At 350 °C, strain values were generally lower and more stable across the cycles, further supporting the presence of thermal recovery mechanisms at elevated temperatures.

Residual stress analysis using X-ray diffraction supported these interpretations. Residual stress increased with the number of ARB cycles and was more prominent at lower temperatures, peaking at over 138 MPa at 250 °C after 3 cycles. In contrast, at 350 °C, residual stress levels remained significantly lower, indicating that heat facilitates stress relaxation. These findings are consistent with earlier reports on SPD-processed magnesium alloys, where increased dislocation density at low temperatures leads to higher internal stresses. To further evaluate internal strain, neutron diffraction was employed. This technique, with its high penetration depth, provided 3-dimensional information about strain distribution. The measurements confirmed compressive strain in all directions after the first cycle at both 250 °C and 350 °C, suggesting uniform deformation. However, in the fourth cycle at 250 °C, anisotropy in the strain became apparent, with some directions exhibiting positive strain. This directional variation may reflect the evolution of texture and partial relaxation within specific grain orientations. The neutron diffraction results corroborated the XRD findings, indicating reorientation toward (004) and (021) planes and emphasizing the contribution of ARB in tailoring crystallographic alignment.

These results align with previous ECAP studies on AZ31 alloys, which found that lower processing temperatures correlate with higher residual stress and enhanced corrosion susceptibility. Such connections emphasize the need to consider not only the mechanical implications of ARB but also its potential impact on environmental stability, especially for applications where corrosion resistance is critical. Overall, the findings confirm that ARB parameters-temperature and cycle count-govern the balance between refinement, texture development, and stress relaxation in magnesium. These insights provide guidance for tailoring processing strategies in future SPD research [38-40].

Conclusions

This study demonstrates that the Accumulative Roll Bonding (ARB) process effectively refines the microstructure and induces residual stress in pure magnesium. The most refined structure was achieved in sample Mg 3A (250 °C, 3 cycles), with a grain size of 6.591 μm, residual stress of 138.275 MPa, and lattice strain of 0.21816%. These results highlight ARB's capacity to generate compressive deformation and enhance structural uniformity. The temperature and number of cycles significantly influence the outcomes. Processing at 250 °C offers superior grain refinement, while 350 °C provides stress relaxation but less refinement. Grain coarsening observed beyond the third cycle suggests a limit to ARB's effectiveness. X-ray and neutron diffraction analyses confirmed texture evolution and internal strain redistribution during ARB. Overall, ARB at 250 °C for up to 3 cycles is optimal for improving magnesium's microstructure and residual stress profile. Beyond summarizing the results, these findings have broader implications. Scientifically, they demonstrate that the combined use of XRD and neutron diffraction offers a powerful multiscale approach to link surface and bulk structural changes in magnesium - a

novelty rarely applied in ARB studies. Practically, the establishment of 250 °C as the optimal processing condition provides guidance for tailoring grain refinement and residual stress to improve mechanical reliability. This is particularly relevant for lightweight structural components where fatigue resistance and dimensional stability are critical. The insights gained from this work can therefore inform both future research in severe plastic deformation mechanisms and the development of processing strategies for magnesium-based alloys in engineering applications. These insights are valuable for advancing SPD techniques in structural applications. A key novelty of this work is the integrated use of XRD and neutron diffraction, which provided complementary perspectives from surface to bulk, offering a new framework for studying residual stress evolution in pure magnesium.

Acknowledgements

We extend our gratitude to the Program Riset dan Inovasi untuk Indonesia Maju (RIIM), an initiative by Lembaga Pengelola Dana Pendidikan (LPDP) and Badan Riset dan Inovasi Nasional (BRIN), Indonesia for their support and funding under the RIIM Gelombang 3 program. This backing was pivotal in facilitating the research activities and accomplishing the goals set forth in this study. We also acknowledge the insightful evaluations and continuous encouragement provided by the Deputy for Research Facilities and Innovation, which have significantly contributed to the enrichment of our work. Our sincere thanks are also due to everyone involved in the administrative and operational support, which has been indispensable throughout the duration of this project.

Declaration of generative AI in scientific writing

The authors declare that generative AI tools were used only to improve the readability and language of the manuscript. These tools were applied with full human oversight and control. The authors remain fully responsible for all scientific content, analysis, and conclusions presented in the paper. No AI tools were listed as authors or co-authors in this work.

CRediT author statement

Muhammad Rifai: Conceptualization, Methodology, Investigation, Writing - original draft, Funding acquisition; **Muhammad Ivan Pratama**: Investigation, Formal analysis; **Azza Alifa Muhammad**: Writing - Reviewing and Editing; **Ahadi Damar Prasetya**: Writing - Reviewing and Editing, Visualization; **Mujamilah**: Supervision, Validation; **Frida Iswinning Diah**: Investigation, Formal Analysis; **Agus Dwiatmaja**: Investigation; **Fajar Sidik Permana**: Investigation; **Kurnia Wibowo**: Resources; **Suharni**: Validation; **Taufik**: Investigation, Formal Analysis; **Emy Mulyani**: Investigation, Formal Analysis; **Ihwanul Aziz**: Validation, Writing - Reviewing and Editing.

References

[1] I Antoniac, M Miculescu, V Mănescu, A Stere, PH Quan, G Păltânea, A Robu and K Earar. Magnesium-based alloys used in orthopedic surgery. *Materials* 2022; **15(3)**, 1148.

[2] A Bordbar-Khiabani, B Yarmand and M Mozafari. Emerging magnesium-based biomaterials for orthopedic implantation. *Emerging Materials Research* 2019; **8(3)**, 305-319.

[3] S Amukarimi and M Mozafari. Biodegradable magnesium-based biomaterials: An overview of challenges and opportunities. *MedComm* 2021; **2(2)**, 123-144.

[4] G Vincze, FJP Simões and MC Butuc. Asymmetrical rolling of aluminum alloys and steels. *Metals* 2020; **10(9)**, 1126.

[5] S Seetharaman, D Sankaranarayanan and M Gupta. Magnesium-based temporary implants: Potential, current status, applications, and challenges. *Journal of Functional Biomaterials* 2023; **14(6)**, 324.

[6] J Wu, X Cheng, J Wu, Junyu Chen and X Pei. The development of magnesium-based biomaterials in bone tissue engineering: A review. *Journal of Biomedical Materials Research Part B: Applied Biomaterials* 2024; **112(1)**, e35326.

[7] FZ Akbarzadeh, M Sarraf, ER Ghomi, VV Kumar, M Salehi, S Ramakrishna and S Bae. A state-of-the-art review on recent advances in the fabrication and characteristics of magnesium-based alloys in biomedical applications. *Journal of Magnesium and Alloys* 2024; **12(7)**, 2569-2594.

[8] Z Wu, R Ahmad, B Yin, S Sandlöbes and WA Curtin. Mechanistic origin and prediction of

enhanced ductility in magnesium alloys. *Science* 2018; **359(6374)**, 447-452.

[9] C Chen, D Han, M Wang, S Xu, T Cai, S Yang, F Shi, B Beausir and LS Toth. High strength and high ductility of Mg-10Gd-3Y alloy achieved by a novel extrusion-shearing process. *Journal of Alloys and Compounds* 2022; **931**, 167498.

[10] G Wu, X Tong, R Jiang and W Ding. Grain refinement of as-cast Mg-RE alloys: Research progress and future prospect. *Acta Metallurgica Sinica* 2022; **58(4)**, 385-399.

[11] Z Fan and F Gao. Grain initiation and grain refinement: An overview. *Metals* 2022; **12(10)**, 1728.

[12] P Peng, H Xue, J She, J Zhang, A Tang, S Long, C Zhang, Q Yang and F Pan. Ultrafine-grained Mg alloy: Preparation, properties, design strategy. *Journal of Materials Research and Technology* 2024; **29**, 4480-4504.

[13] S Harjo, W Gong and T Kawasaki. Stress evaluation method by neutron diffraction for HCP-structured magnesium alloy. *Quantum Beam Science* 2023; **7(4)**, 32.

[14] E Rabkin, V Skripnyuk and Y Estrin. Ultrafine-grained magnesium alloys for hydrogen storage obtained by severe plastic deformation. *Frontiers in Materials* 2019; **6**, 240.

[15] P Mansoor and SM Dasharath. Microstructural and mechanical properties of magnesium alloy processed by severe plastic deformation (SPD) - A review. *Materials Today: Proceedings* 2020; **20(2)**, 145-154.

[16] A Abbas and SJ Huang. Investigation of severe plastic deformation effects on microstructure and mechanical properties of WS2/AZ91 magnesium metal matrix composites. *Materials Science and Engineering: A* 2020; **780**, 139211.

[17] Z Zhang, J Wang, Q Zhang, S Zhang, Q Shi and H Qi. Research on grain refinement mechanism of 6061 aluminum alloy processed by combined SPD methods of ECAP and MAC. *Materials* 2018; **11(7)**, 1246.

[18] CLP Silva, RB Soares, PHR Pereira, RB Figueiredo, VFC Lins and TG Langdon. The effect of high-pressure torsion on microstructure, hardness and corrosion behavior for pure magnesium and different magnesium alloys. *Advanced Engineering Materials* 2019; **21(3)**, 1801081.

[19] SM Ghalehbandi, M Malaki and M Gupta. Accumulative roll bonding - a review. *Applied Sciences* 2019; **9(17)**, 3627.

[20] J Guo, W Sun, N Xiang and F Chen. Interfacial bonding and fracture behaviors of AZ63 magnesium alloy sheet processed by accumulative roll bonding. *Materials* 2023; **16(14)**, 4981.

[21] J Guo, J Wang, T Zhang and S Zhang. Microstructure and properties of LZ91 magnesium alloy processed by asynchronous accumulative roll bonding. *Materials Research Express* 2020; **7(12)**, 126513.

[22] Y Pei, Y Gui, T Huang, F Chen, J Guo, S Zhong and Z Song. Microstructure and corrosion behaviors of AZ63 magnesium alloy fabricated by accumulative roll bonding process. *Materials Research Express* 2020; **7**, 066525.

[23] JF Nie, KS Shin and ZR Zeng. Microstructure, deformation, and property of wrought magnesium alloys. *Metallurgical and Materials Transactions A* 2020; **51**, 6045-6109.

[24] Q Sun, D Zhang, X Tong, J Lin, Y Li and C Wen. Mechanical properties, corrosion behavior, and cytotoxicity of biodegradable Zn/Mg multilayered composites prepared by accumulative roll bonding process. *Acta Biomaterialia* 2024; **173**, 509-525.

[25] LDCG Púa, JCR Montenegro, AMF Reyes, HZ Rodríguez and VNP Méndez. Biomaterials for orthopedic applications and techniques to improve corrosion resistance and mechanical properties for magnesium alloy: A review. *Journal of Materials Science* 2023; **58**, 3879-3908.

[26] L Sun, F Li, YQ Li, C Li and AX Zhang. Refining grain structure and improving elongation properties in AZ31 magnesium alloy sheets using hard plate accumulative roll bonding. *Materials Science and Engineering: A* 2023; **887**, 145774.

[27] G Han, HK Park, HK Kim and TS Jun. Local and global deformation behaviour in rolled pure magnesium sheets at room temperature under different strain rates. *Materials Science and Engineering: A* 2019; **762**, 138110.

[28] Z Zeng, M Zhou, P Lynch, F Mompiou, Q Gu, M Esmaily, Y Yan, Y Qiu, S Xu, H Fujii, C Davies, JF Nie and N Birbilis. Deformation modes during

room temperature tension of fine-grained pure magnesium. *Acta Materialia* 2021; **206**, 116648.

[29] Z Zhang, L Yuan, D Shan and B Guo. The quantitative effects of temperature and cumulative strain on the mechanical properties of hot-extruded AZ80 Mg alloy during multi-directional forging. *Materials Science and Engineering: A* 2021; **827**, 142036.

[30] D Panda, RK Sabat, S Suwas, VD Hiwarkar and SK Sahoo. Texture weakening in pure magnesium during grain growth. *Philosophical Magazine* 2019; **99(11)**, 1362-1385.

[31] D Vinotha, K Raghukandan, UTS Pillai and BC Pai. Grain refining mechanisms in magnesium alloys - an overview. *Transactions of the Indian Institute of Metals* 2010; **62**, 521-532.

[32] H Mirzadeh. Grain refinement of magnesium alloys by dynamic recrystallization (DRX): A review. *Journal of Materials Research and Technology* 2023; **25**, 7050-7077.

[33] H Shao, L He, H Lin and HW Li. Progress and trends in magnesium-based materials for energy-storage research: A review. *Energy Technology* 2018; **6(3)**, 445-458.

[34] H Zhou, B Liang, H Jiang, Z Deng and K Yu. Magnesium-based biomaterials as emerging agents for bone repair and regeneration: From mechanism to application. *Journal of Magnesium and Alloys* 2021; **9(3)**, 779-804.

[35] Z Shu-yan, G Jian-bo, W Shu-wen and P Sanjooram. Application of neutron diffraction in residual stress analysis. *Failure Analysis and Prevention* 2021; **16(1)**, 60-69.

[36] A Baczmański, P Kot, S Wroński, M Wróbel, M Wroński, J Pilch, M Muzyka, K Wierzbanowski, Y Zhao, LL Joncour, M François and B Panicaud. Direct diffraction measurement of critical resolved shear stresses and stress localisation in magnesium alloy. *Materials Science and Engineering: A* 2021; **801**, 140400.

[37] Y Nie, J Dai, X Li and X Zhang. Recent developments on corrosion behaviors of Mg alloys with stacking fault or long period stacking ordered structures. *Journal of Magnesium and Alloys* 2021; **9(4)**, 1123-1146.

[38] K Wei, R Hu, D Yin, L Xiao, S Pang, Y Cao, H Zhou, Y Zhao and Y Zhu. Grain size effect on tensile properties and slip systems of pure magnesium. *Acta Materialia* 2021; **206**, 116604.

[39] E Karakulak. A review: Past, present and future of grain refining of magnesium castings. *Journal of Magnesium and Alloys* 2019; **7(3)**, 355-369.

[40] DR Liu, H Zhao and L Wang. Numerical investigation of grain refinement of magnesium alloys: Effects of cooling rate. *Journal of Physics and Chemistry of Solids* 2020; **144**, 109486.